IEEE Access
Multidisciplinary | Rapid Review | Open Access Journal

Received 14 June 2022, accepted 4 July 2022, date of publication 7 July 2022, date of current version 19 July 2022.

Digital Object Identifier 10.1109/ACCESS.2022.3189369

RESEARCH ARTICLE

Accurate Detection of Chylous Blood Levels by Deep Learning

QING QIAN[1,2], WENCHANG XU[1], WENXIANG LI[1], BIAO WANG[1,2], LEI WANG[1], AND QUNGANG ZHOU[3]

[1]Suzhou Institute of Biomedical Engineering and Technology, Chinese Academy of Sciences, Suzhou 215163, China
[2]University of Science and Technology of China, Hefei 260026, China
[3]Suzhou Blood Center, Suzhou 215006, China

Corresponding authors: Wenchang Xu (xuwc@sibet.ac.cn) and Lei Wang (wanglei@sibet.ac.cn)

ABSTRACT Chylous blood, a kind of abnormal blood with an increasing proportion, should be excluded from unpaid blood donation. Therefore, it is important to determine the level of chylous blood, to judge that whether blood is applicable. In this manuscript, the image was preprocessed by the image acquisition device of the background board. Moreover, an improved ResNet-50 neural network model of chylous blood level based on images was established which decreased the parameters by about 44.5%, and thus greatly reducing the amount of calculation and improving the ability of the network to distinguish image details. It was found that the average values of precision, sensitivity, and F1-Score of the model were all above 0.95. Furthermore, the accuracy of the 5-level determination of the plasma chylous blood level was above 0.95. Compared with manual judgment, this method significantly improved the efficiency and accuracy of detection.

INDEX TERMS Chylous blood, ResNet, deep learning, image processing.

I. INTRODUCTION

Chylous blood is a kind of blood obtained from patients with chylomicronemia syndrome [1]–[3]. Such blood is often milky white or turbid due to massive accumulation of chylomicrons. Moreover, it will cause undesirable reactions to the recipient by donating blood, and affect the detection of other blood indexes such as alanine aminotransferase (ALT) and hemoglobin [4]–[7]. Severely chylous blood should be forbidden to be used in clinic. Therefore, it is more important to quickly determine whether the blood of donors is chylous blood, which is difficult now.

In order to identify chylous blood, the instruments including enzyme-labeled instrument [8], automatic enzyme immunoassay analyzer [9], chemistry analyzer [10], Ultraviolet-visible spectrophotometry [11], and other large optical instruments have been applied. Although the level of chylous blood can be determined by these instruments, users need to take the blood from the blood bag to pass these instruments, which is inconvenient to operate. Moreover, these instruments are expensive and inconvenient to operate, and are therefore not suitable for rapid testing. Because of the special requirements of time and space for blood collection, most of doctors only rely on the naked eyes and experiences to judge the level of chylous blood [12], [13]. However, there are obviously individual differences by this method, which can easily lead to the waste of blood or repeated centrifugation [14].

Similar problems occurred in other biomedical detections conducted by computed tomography (CT), magnetic resonance imaging (MRI), positron emission tomography (PET) ultrasound, and X-ray. Medical imaging interpretation is primarily performed by radiologists and clinicians. However, there is considerable instability in the experience of physicians. Therefore, improvements by machine learning techniques are in demand be help physicians with computer assistance. Recently, deep neural networks have been gradually applied to sophisticated medical image detection. For example, Gomez-Valverde *et al.* [15] proposed methods of Convolution Neural Network (CNN) and Visual Graphics Generator (VGG19) to automatically classify color fundus images for glaucoma. It was generally believed that the accuracy would be improved if these layers were simply stacked to form a deep network. However, we observed

The associate editor coordinating the review of this manuscript and approving it for publication was Vishal Srivastava.

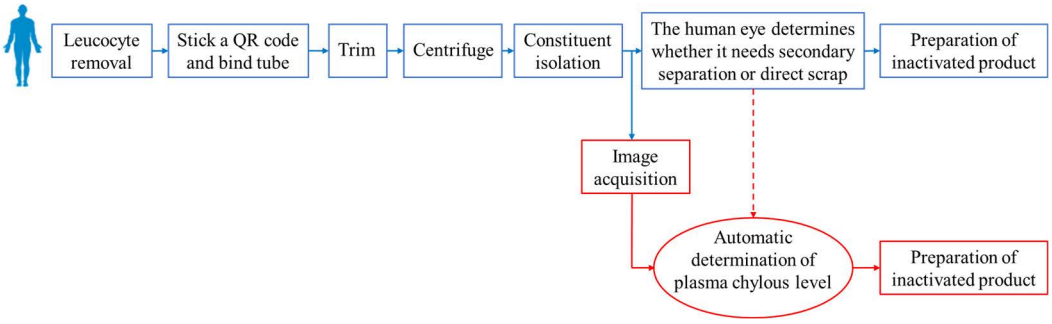

FIGURE 1. Basic process of blood preparation.

a decrease in accuracy when training a deeper network. The deep residual network (Resnet) solved this problem by both detecting the image details and maintaining a high accuracy. Chen *et al.* [16] used the VoxResNet network to accurately segment brain images. Sarwinda *et al.* [17] used Resnet to classify and recognize colorectal cancer medical images, whose accuracy was more than 80%. Yu *et al.* [18] detected breast abnormalities in medical images by improved Resnet-50 model. To improve prediction accuracy, they created a new data augmentation framework called SCDA (Scaling and Contrast limited adaptive histogram equalization Data Augmentation). In other words, they added a new data augmentation framework after ResNet-50 model instead of changing the network structure.

At present, there have been few literatures on the classification of chylous blood, which is mainly carried out by the staff of blood center according to the industry standard WS/T 550-2017 [19]. Human factors lead to subjective results. Since the chylous blood classification needs a large amount of medical data as early support, this research is closer to practical application. By cooperation with the blood center, we have obtained a large number of data, which provides support for us to classify chyle blood by using the deep learning method. Because the chylous plasma images of different level studied in this paper are only slightly different, resulting in the decrease of recognition accuracy. ResNet network can obtain deep-seated features. Therefore, it is necessary to improve ResNet-50 model according to the characteristics of the data set in this paper.

This paper intended to use an image-based deep neural network to determine the degree of plasma chyle. An improved Resnet-50 neural network model were established, and the results indicated a fact that the accuracy of the 5-level determination of the plasma chylous blood level can reach 0.95. This innovative method provided a new idea for blood engineering by breaking through the inconvenience of traditional methods and the disadvantages of subjective differences.

II. DATA ACQUISITION

The blood centers are responsible for the collection and supply of clinical blood, as well as the blood transfusion in hospitals and the business guidance for primary blood centers. The data in this paper came from the blood preparation process after centrifugation and they were in the stage of the human-eye judging whether they needed secondary separation or direct scrap [20]. The general process of blood preparation was shown in Figure 1.

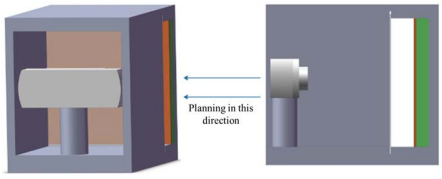

FIGURE 2. Overall diagram of the collection device.

TABLE 1. Camera parameter table.

Model	C33
Camera resolution	1920×1080dpi
Sensor	CMOS
Max FPS	30

A. COLLECTION DEVICE

The centrifuged blood bag was placed in a self-designed light-shielding image acquisition device without taking out the blood from the blood bag. The overall schematic diagram of the device was shown in Figure 2. The left picture was the front view of the device, and the right picture was the side plan view.

In order to ensure the stability of the images taken by the device, a fixed-focus camera of the AONI brand was used in the device. The parameters are shown in Table 1.

The specific method of the experimental device is shown in Figure 3.

Since the difference in plasma color between the 5-level was relatively subtle, we used a multi-wavelength combination of white LED light-emitting panels. The white LED emission spectrum was widely distributed in the visible light field, so the color of plasma in the blood bag was not distorted. The backlight plate of the white light board adopted PC board and optical grade acrylic board, and the light transmittance was more than 93%.

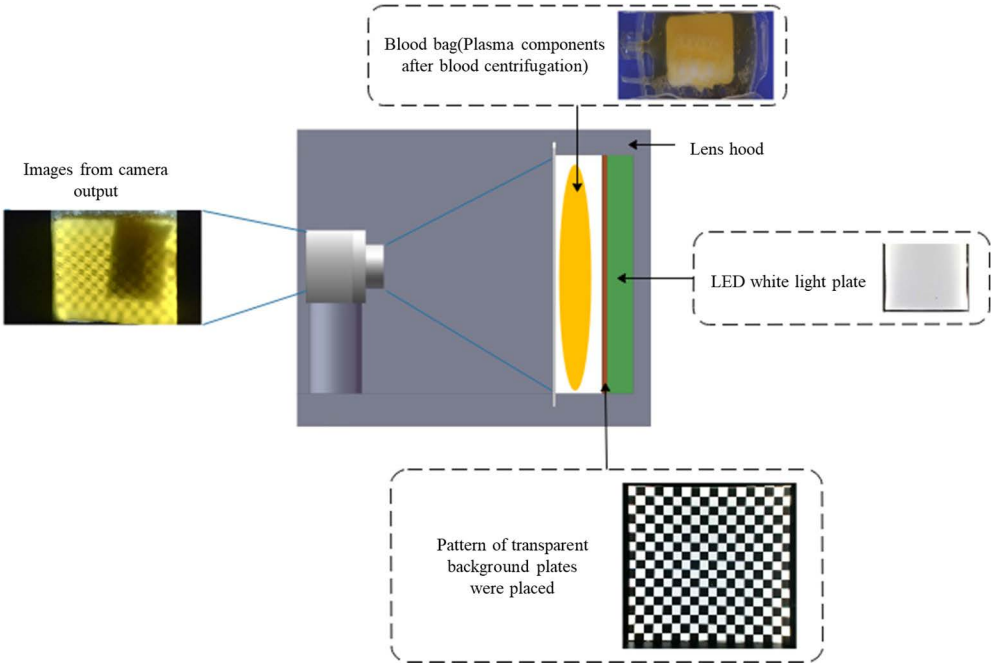

FIGURE 3. Schematic diagram of experimental device.

When the incident light intensity of the white LED light-emitting panel I_0 is constant [21], the greater the intensity of light I_a absorbed, the smaller the intensity of transmitted. Light I_t. I_t / I_0 could represent the ability of light to pass through the medium, which was called light transmittance. When incident light entered the plasma with different level of chylous blood, the transmission of light in the channel was blocked. The reason for this phenomenon was that the light contained a large number of chylomicrons. Therefore, the light stayed in the plasma to be absorbed. On the other hand, the light transmittance was reduced.

In order to avoid the complicated operations such as the use of photometers by front-line blood collection personnel, we designed a style of transparent background boards between the blood bag and the white light-emitting board to better exhibit the light transmittance of plasma with different chylous blood levels, as shown in the Figure 3. Finally, the plasma image received by the camera was used to determine the level of chylous blood through image recognition [22].

B. PLASMA IMAGE ACQUISITION

According to the regulation of WS/T 550-2017, the chylous blood level can be divided into five levels, of which 1 was normal blood and 5 was severe chylous blood. Grade 1 plasma was fresh plasma, which could be directly extracted by cold precipitation, and then frozen to prepare plasma for transmission. Grade 5 plasma belonged to dangerous plasma and was directly discarded. Grade 4 plasma needed to be judged whether it should be discarded. Grade 2 and 3 plasma needed to be further judged whether they could be directly used or be made into virus inactivated plasma. If the time exceeded 6 hours, the plasma should be made into virus inactivated plasma. If the time was within 6 hours, the blood could be extracted by cold precipitation or made into virus inactivated plasma. In this paper, the level of chylous blood was jointly marked by two experienced chief technicians at the Suzhou Central Blood Center. Taking the images with the gird background board an example, the marking results and collection conditions were shown in Table 2.

III. IMAGE PREPROCESSING

Because of the number of images collected for each level was rather small, it was necessary to preprocess the currently collected images in order to ensure the quality and balance of the data set of the model. The preprocessing process is shown in Figure 4.

The picture with original size of 1920 × 1080 and no labels was cut into 100 × 100 pictures. 100 pictures were segmented from the original 1920 pictures by program. Noise removal was done manually. The schematic diagram was shown in Figure 5.

Chylous blood was classified from Grade 1 to Grade 5. Different grades of chylous blood had different sample numbers. For example, there were 30 samples of chylous blood in Grade 1. Different data sets are obtained by image preprocessing of different levels of chylous blood. The dataset was the number segmented from the original 1920 × 1180 image to 100 × 100 images. In each category, the images were randomly arranged and picked, to ensure the credibility of the samples. After the image preprocessing, we obtained a data set of 11, 500 cases of chylous blood level in total.

TABLE 2. Marking results and collection situation.

Level of chylous blood	Number of image acquisition	Image examples
Grade 1	30 cases	
Grade 2	10 cases	
Grade 3	15 cases	
Grade 4	7 cases	
Grade 5	8 cases	

FIGURE 4. Data preprocessing flowchart.

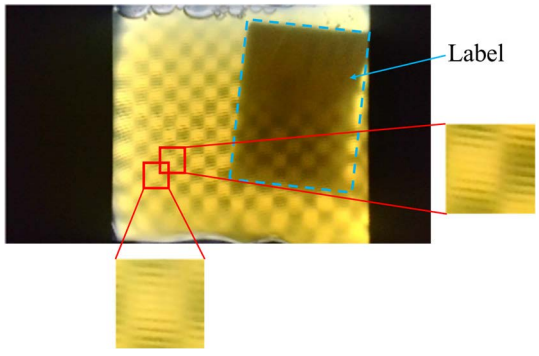

FIGURE 5. Image cutting diagram.

The specific distribution was shown in Table 3. For example, 2000 images were obtained from 7 figures for chylous blood in Grade 4, which were staggered interceptions to ensure the accuracy of deep learning, including some overlapping areas.

TABLE 3. Data set distribution.

Level of chylous blood	Number of image acquisitions	Distribution of datasets
Grade 1	30	3500
Grade 2	10	2000
Grade 3	15	2000
Grade 4	7	2000
Grade 5	8	2000
Total	70	11500

IV. MODEL

This paper proposed an improved deep residual network model. In this model, 7×7 convolution kernel in the first convolution layer of the traditional ResNet-50 model [23]–[25] was replaced with a 5×5 convolution kernel. In general, the 7×7 convolution kernel was regarded as a larger convolution kernel, and it was used to extract larger neighborhood information of the input image. However, the differences between the sharpness of the background plate and the image edge were relatively too subtle to be used in the recognition of chylous blood level. The differences in the characteristics of categories were not significant. In view of the above phenomena, it is necessary to extract more subtle features from the chyle blood image to achieve a more accurate classification of chylous blood level images. Besides, the unimproved 7×7 convolution kernel had $7 \times 7 \times$channels$=49 \times$channels parameters. The parameter numbers of the improved three 5×5 convolution kernels were $5 \times 5 \times$channels$=25 \times$channels, reducing about 44.5% of the parameters. It was concluded that the amount of calculation was greatly reduced, and the network's ability to identify image details was improved.

The interpolation algorithm was applied to the collected data set, which was put into the improved ResNet-50 neural network for training. The improved network diagram was shown in Figure 6.

V. RESULTS AND DISCUSSION

In order to ensure the rationality of the model, this paper used a 5-fold cross-validation method [26] for data training and model verification, as an optimal classification model. Then the model was tested using a test set that was exclusive to the training set, and the final classification model was determined. The 5-fold cross-validation method was shown in Figure 7.

The data set used in this article contained a total of 11500 images of different levels of chyle. After dividing the data set, the training set accounted for 80%, and the test set accounted for 20%. Then the training set was divided into a validation set and a training set according to a 5-fold cross-validation method. The division was shown in Table 4.

In order to verify the rationality of the neural network construction, this paper used the SoftMax cross-entropy loss function to perform Loss analysis on the training set and the test set, as shown in the eqution1:

$$E(t, y) = -\sum_j t_j \log y_i \tag{1}$$

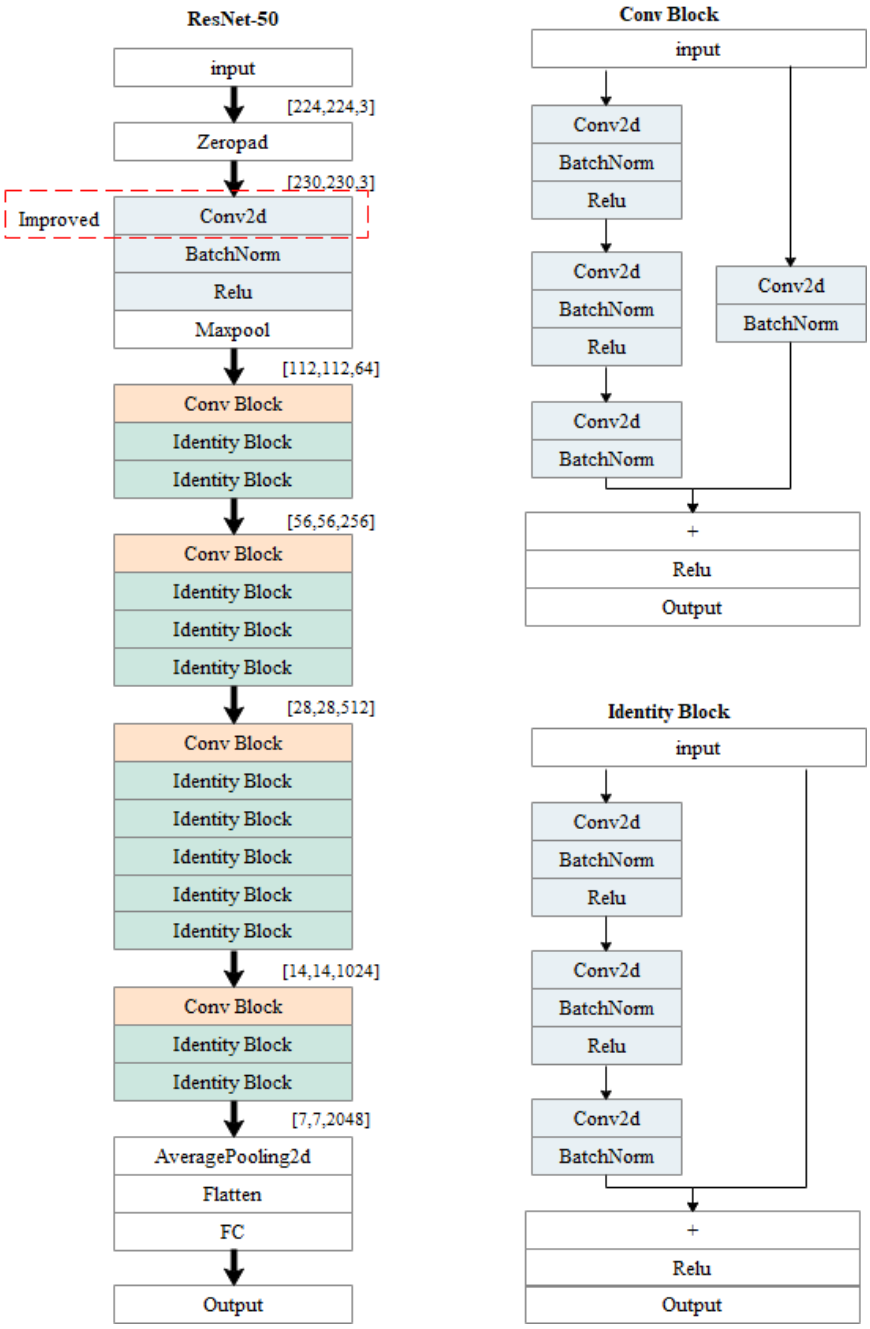

FIGURE 6. Schematic diagram of neural network.

where t and y represented the category label and actual recognition output value of the neural network, respectively. Meanwhile, $y_i$represented the SoftMax loss function:

$$y_i = soft\max\left(z_j\right) = \frac{e^{zj}}{\sum_j e^{zj}} \tag{2}$$

This paper used the improved Resnet-50 neural network model framework built by Keras, and the network model parameter settings were shown in Table 5. The training of this model used NVIDIA Quadro P2200 graphics card with 5g video memory capacity. The training time of the first full epoch of the model was 132 s, and then the time gradually decreased. The training time of the last 150th epoch reached 111 s. The total of time is 16525 s, which is about 4.59 h. The total number of parameters in all layers of the model was 25017837. Table 5 judged and adjusted parameters through the loss curves in Figure 8a). The two loss curves of the training set and the verification set could show several states of over fitting, under fitting and just fitting of the model. At first, you need to select optimizer, and

TABLE 4. Data set distribution.

Total	*training set（80%）（5 fold cross validation）*		*test set（20%）*
	training set（80%）	Validation set（20%）	
11500	7360	1840	2300

TABLE 5. Parameters of improved Resnet-50 neural network model.

Neural network models	Improved ResNet-50
parameter	Epoch=150
	Batch size=32
	Learning rate=0.014
	Decay=0.001
	Optimizer=SGD (Stochastic gradient descent)

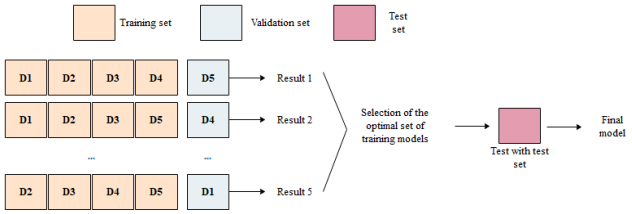

FIGURE 7. Process of five-fold cross-validation method.

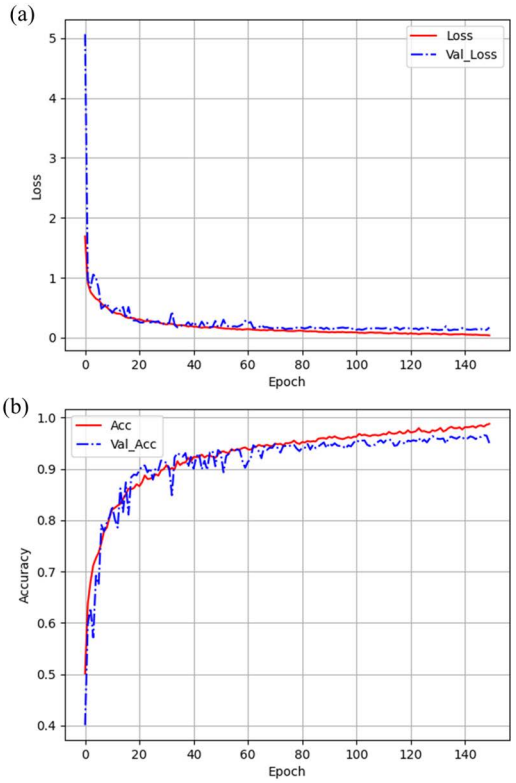

FIGURE 8. Loss curve and accuracy curve of the improved Resnet-50 model. (a) is the Loss curve, (b) is the accuracy curve.

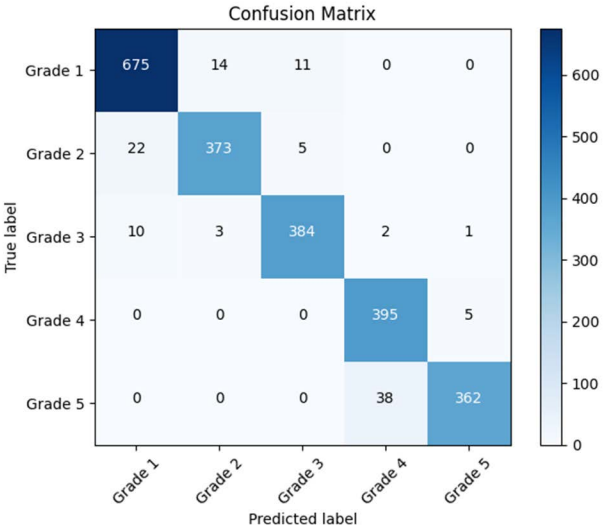

FIGURE 9. Confusion matrix of the test set.

then adjust the learning rate and decay to make the model in the just fitting state. At this time, the model had strong generalization ability. Finally, an appropriate batch size was determined according to the number of data sets. When the two loss curves were stable, the epoch would be reduced to obtain the existing model parameters in Table 5. All parameters were optimized according to the characteristics of the data set.

The group with better training effect was selected among the 5 training models with 5-fold cross-validation. The results of Loss curve and Accuracy (ACC) curve through the improved Resnet-50 model were analyzed. The results were shown in Figure 8.

It could be seen from Figure 8a that the Loss curve of the training set was almost parallel to the Loss curve of the validation set, and the difference between the two lines was small. These phenomena indicated that the Resnet-50 neural network model finally tended to stay in a stable state. Compared with the Acc curve obtained for the training set (Figure 8b,) and the Acc curve obtained for the validation set, the model have not reached the over-fitting state. Thus, the classification effect should be good. The average accuracy of the validation set curve was about 0.95.

Subsequently, we applied the model to the test set, and the data distribution of Grade1, Grade2, Grade3, Grade4, and Grade5 in the test set were 700 cases, 400 cases, 400 cases, 400 cases, and 400 cases, respectively. The confusion matrix was shown in Figure 9.

In order to better evaluate the model, this paper introduced the three indexes including precision, sensitivity [27] and accuracy. The expression formulas were as follows:

$$precision = \frac{TP}{TP + FP} \tag{3}$$

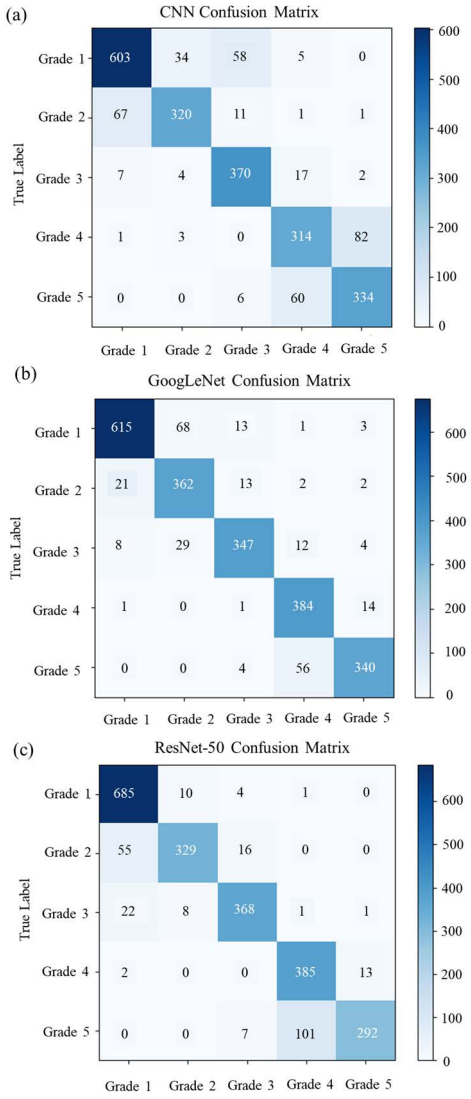

FIGURE 10. Schematic diagram of confusion matrix. (a) is the CNN confusion matrix, (b) is the GoogLeNet confusion matrix, and (c) is the traditional ResNet-50 confusion matrix.

TABLE 6. Evaluation index of improved Resnet-50 neural network.

	Precision	recall	F1-score	Support
Grade 1	0.95	0.96	0.96	700
Grade 2	0.96	0.93	0.94	400
Grade 3	0.96	0.96	0.96	400
Grade 4	0.91	0.99	0.95	400
Grade 5	0.98	0.91	0.94	400
Average	0.95	0.95	0.95	2300
Accuracy		0.95		2300

$$sensitivity = \frac{TP}{TP + FN} \tag{4}$$

$$accuracy = \frac{TP + TN}{TP + TN + FP + FN} \tag{5}$$

TABLE 7. Comparison and analysis table of the three models.

Model	Lable	Precision	recall	F1-score
CNN	Grade 1	0.89	0.86	0.88
	Grade 2	0.89	0.80	0.84
	Grade 3	0.83	0.93	0.88
	Grade 4	0.79	0.79	0.79
	Grade 5	0.80	0.83	0.82
	Average	0.84	0.84	0.84
	Accuracy		0.84	
GoogLeNet	Grade 1	0.95	0.88	0.91
	Grade 2	0.79	0.91	0.84
	Grade 3	0.92	0.87	0.89
	Grade 4	0.84	0.96	0.90
	Grade 5	0.94	0.85	0.89
	Average	0.89	0.89	0.89
	Accuracy		0.89	
ResNet-50	Grade 1	0.90	0.98	0.94
	Grade 2	0.95	0.82	0.88
	Grade 3	0.93	0.92	0.93
	Grade 4	0.79	0.96	0.87
	Grade 5	0.95	0.73	0.83
	Average	0.90	0.88	0.89
	Accuracy		0.90	
Proposed (Improved ResNet-50)	Grade 1	0.95	0.96	0.96
	Grade 2	0.96	0.93	0.94
	Grade 3	0.96	0.96	0.96
	Grade 4	0.91	0.99	0.95
	Grade 5	0.98	0.91	0.94
	Average	**0.95**	**0.95**	**0.95**
	Accuracy		**0.95**	

where *TP* represented the number of correct classifications, *FP* represented the number of other categories classified into this category, and *FN* represented the number of incorrect classifications of this category. Combining these two evaluation parameters, the F1-Score evaluation index was introduced. Since accuracy and sensitivity were equally important, we set the value of β in the F1-Score calculation formula to 1. The calculation method was as follows:

$$F1 - score(\beta = 1) = \frac{2 \times precision \times sensitivity}{precision + sensitivity} \tag{6}$$

F1-Score value ranged from 0 to 1. The higher the F1-Score value, the better the classification effect of the model. The evaluation indicators of the neural network were shown in Table 6.

GoogLeNet is a new in-depth learning structure which was proposed in 2014. Its feature is to add inception module to improve the training results, which plays an important role in the field of image classification. Based on the

image-based study of the intelligent judgment algorithm for the grading of plasma chyle, the authors have tested the CNN model [28]–[30], GoogLeNet, and the traditional Resnet-50 model at the same time. The confusion matrix of the three models was shown in Figure 10.

For the three models, the indicators of precision, sensitivity and F1-Score were calculated, which were used for the comparison among the three models. The comparison date was shown in Table 7.

As shown in Table 7, the classification accuracy of the CNN network model was 0.84 and the value of GoogLeNet model reached 0.89. However, CNN model had poor accuracy at level 4 and GoogLeNet model had poor accuracy at level 2. Compared with CNN and GoogLeNet models, the traditional ResNet-50 model had higher overall accuracy, but still had poor accuracy in level 2. The improved Resnet-50 network model performed well in all the 5 levels of blood chloremia. The averaged precision and recall indicators were around 0.95, while the F1-score value was 0.95. The overall accuracy rate reached 0.95. This improved model exhibited a good ability to intelligently determine the degree of blood chyle.

VI. CONCLUSION

Considering that the traditional method for determining the level of chylous blood was inconvenient to operate and subjectively differed greatly, this paper proposed a new intelligent method for determining the degree of blood chyle, which reduced labor costs and man-made operating errors. This method collected images with a background plate on the blood bag after the initial centrifugation, and used the improved Resnet-50 neural network model to classify chylous blood level according to the images. It had a good performance in the determination of the five levels of blood chyle, with the overall accuracy of determination reaching 0.95, thus demonstrating a good ability to intelligently determine the blood chyle. This method also provided new ideas and methods for blood engineering.

ACKNOWLEDGMENT

The authors would like to thank the editor for their support and the anonymous reviewers for their valuable suggestions.

REFERENCES

[1] D. A. Leaf, "Chylomicronemia and the chylomicronemia syndrome: A practical approach to management," *Amer. J. Med.*, vol. 121, no. 1, pp. 2–10, Jan. 2008.

[2] E. Stroes, P. Moulin, K. G. Parhofer, V. Rebours, J.-M. Löhr, and M. Averna, "Diagnostic algorithm for familial chylomicronemia syndrome," *Atherosclerosis Supplements*, vol. 23, pp. 1–7, Jan. 2017.

[3] S. J. Baek, S. H. Kim, J. M. Kwak, and J. Kim, "Incidence and risk factors of chylous ascites after colorectal cancer surgery," *Amer. J. Surg.*, vol. 206, no. 4, pp. 555–559, Oct. 2013.

[4] J. Sesti, J. Luker, J. Decker, and S. Paul, "Modified blood patch used to treat a high output chyle leak after McKeown esophagectomy," *Ann. Thoracic Surg.*, vol. 109, no. 6, pp. e401–e402, Jun. 2020.

[5] M. Raturi and A. Kusum, "Deciphering the reasons for milky-white blood donor plasma," *Transfusion Clinique Biologique*, vol. 27, no. 4, pp. 259–261, Nov. 2020.

[6] M. Raturi, A. Ahlawat, M. Kala, A. Kusum, and A. Sahrawat, "Strawberry milky-white blood donor's plasma: Signaling uncontrolled diabetic lipemia," *Transfusion Clinique Biologique*, vol. 28, no. 3, pp. 291–292, Aug. 2021.

[7] N. Agnihotri and L. Kumar, "Turbid plasma donations: Need for quantification," *Asian J. Transfusion Sci.*, vol. 8, no. 2, pp. 78–79, Jul. 2014.

[8] H. Wakayama, T. G. Henares, K. Jigawa, S.-I. Funano, K. Sueyoshi, T. Endo, and H. Hisamoto, "Design of a single-step immunoassay principle based on the combination of an enzyme-labeled antibody release coating and a hydrogel copolymerized with a fluorescent enzyme substrate in a microfluidic capillary device," *Lab Chip*, vol. 13, no. 22, pp. 4304–4307, 2013.

[9] Z. Shang, X. Zhou, C. Li, and S.-B. Tsai, "A study on micropipetting detection technology of automatic enzyme immunoassay analyzer," *Sci. Rep.*, vol. 8, no. 1, p. 5757, Apr. 2018.

[10] B. Flatland, L. C. Breickner, and M. M. Fry, "Analytical performance of a dry chemistry analyzer designed for in-clinic use," *Vet. Clin. Pathol.*, vol. 43, no. 2, pp. 206–217, Jun. 2014.

[11] Q. Lai, S. Zhu, X. Luo, M. Zou, and S. Huang, "Ultraviolet-visible spectroscopy of graphene oxides," *AIP Adv.*, vol. 2, no. 3, Sep. 2012, Art. no. 032146.

[12] R. Bhardwaj, H. Vaziri, A. Gautam, E. Ballesteros, D. Karimeddini, and G. Y. Wu, "Chylous ascites: A review of pathogenesis, diagnosis and treatment," *J. Clin. Transl. Hepatol.*, vol. 6, no. 1, pp. 105–113, Mar. 2018.

[13] G. Tulunay, I. Ureyen, T. Turan, A. Karalok, D. Kavak, N. Ozgul, R. Ocalan, O. L. Tapisiz, N. Boran, and M. F. Kose, "Chylous ascites: Analysis of 24 patients," *Gynecolog. Oncol.*, vol. 127, no. 1, pp. 191–197, Oct. 2012.

[14] K. Peffer, W. L. de Kort, E. Slot, and C. J. Doggen, "Turbid plasma donations in whole blood donors: Fat chance?" *Transfusion*, vol. 51, no. 6, pp. 1179–1187, Jun. 2011.

[15] J. J. Gómez-Valverde, A. Antón, G. Fatti, B. Liefers, A. Herranz, A. Santos, C. I. Sánchez, and M. J. Ledesma-Carbayo, "Automatic glaucoma classification using color fundus images based on convolutional neural networks and transfer learning," *Biomed. Opt. Exp.*, vol. 10, no. 2, pp. 892–913, Feb. 2019.

[16] H. Chen, Q. Dou, L. Yu, J. Qin, and P.-A. Heng, "VoxResNet: Deep voxelwise residual networks for brain segmentation from 3D MR images," *NeuroImage*, vol. 170, pp. 446–455, Apr. 2018.

[17] D. Sarwinda, R. H. Paradisa, A. Bustamam, and P. Anggia, "Deep learning in image classification using residual network (ResNet) variants for detection of colorectal cancer," *Proc. Comput. Sci.*, vol. 179, pp. 423–431, Jan. 2021.

[18] X. Yu, C. Kang, D. S. Guttery, S. Kadry, Y. Chen, and Y.-D. Zhang, "ResNet-SCDA-50 for breast abnormality classification," *IEEE/ACM Trans. Comput. Biol. Bioinf.*, vol. 18, no. 1, pp. 94–102, Jan. 2021.

[19] *Guidelines on Quality Monitoring of Whole Blood and Blood Components*, Standard WS/T 550-2017, Health Industry Standard of the People's Republic of China, 2017.

[20] T. Sood, R. K. Bedi, and K. Mittal, "Discolored blood and blood components: A dilemma for transfusion specialists," *Transfusion Apheresis Sci.*, vol. 50, no. 2, pp. 255–259, Apr. 2014.

[21] X. Feng, W. Xu, Q. Han, and S. Zhang, "LED light with enhanced color saturation and improved white light perception," *Opt. Exp.*, vol. 24, no. 1, pp. 573–585, Jan. 2016.

[22] M. Kompany-Zareh, H. Tavallali, N. Shakernasab, M. Khoshkam, and E. Shamsdin, "Image based kinetic determination of iron(III) in blood samples using a CCD camera," *Reaction Kinetics, Mech. Catal.*, vol. 107, no. 1, pp. 49–61, Oct. 2012.

[23] H. Wang, S. Li, L. Song, and L. Cui, "A novel convolutional neural network based fault recognition method via image fusion of multi-vibration-signals," *Comput. Ind.*, vol. 105, pp. 182–190, Feb. 2019.

[24] T. A. Salih, A. J. Ali, and M. N. Ahmed, "Deep learning convolution neural network to detect and classify tomato plant leaf diseases," *OALib*, vol. 7, no. 5, pp. 1–12, 2020.

[25] K. He, X. Zhang, S. Ren, and J. Sun, "Deep residual learning for image recognition," in *Proc. IEEE Conf. Comput. Vis. Pattern Recognit. (CVPR)*, Jun. 2016, pp. 770–778.

[26] J. Wei and H. Chen, "Determining the number of factors in approximate factor models by twice K-fold cross validation," *Econ. Lett.*, vol. 191, Jun. 2020, Art. no. 109149.

[27] L. D. Sharma and R. K. Sunkaria, "Myocardial infarction detection and localization using optimal features based lead specific approach," *IRBM*, vol. 41, no. 1, pp. 58–70, 2020.

[28] M. O. Khairandish, M. Sharma, V. Jain, J. M. Chatterjee, and N. Z. Jhanjhi, "A hybrid CNN-SVM threshold segmentation approach for tumor detection and classification of MRI brain images," *IRBM*, vol. 2021, pp. 1–10, Jun. 2021.
[29] H. M. Rai, K. Chatterjee, and S. Dashkevich, "Automatic and accurate abnormality detection from brain MR images using a novel hybrid UnetResNext-50 deep CNN model," *Biomed. Signal Process. Control*, vol. 66, Apr. 2021, Art. no. 102477.
[30] L. Xu, K. Zhang, G. Yang, and J. Chu, "Gesture recognition using dual-stream CNN based on fusion of sEMG energy kernel phase portrait and IMU amplitude image," *Biomed. Signal Process. Control*, vol. 73, Mar. 2022, Art. no. 103364.

QING QIAN was born in 1985. He received the master's degree in mechanical electronic engineering from Shandong University, in 2010. He is currently an Associate Research Fellow. His research interests include optoelectronic measurement, control technology, and maldi-TOF mass spectroscopy.

WENCHANG XU was born in 1993. She received the master's degree in mechanical electronic engineering from the University of Chinese Academy of Sciences, in 2018. Her research interests include optimization algorithm and collaborative decision-making technology based on big data analysis, and the application of deep learning on medical.

WENXIANG LI was born in 1995. He received the master's degree in mechanical engineering from Shandong University, in 2020. He is currently an Assistant Researcher with the Suzhou Institute of Biomedical Engineering and Technology, Chinese Academy of Sciences. His main research interests include mechanical structure design and medical device development.

BIAO WANG was born in 1998. He received the bachelor's degree in communication engineering from the Nanjing University of Science and Technology. He is currently pursuing the master's degree with the University of Science and Technology of China. His current research interests include image processing and artificial intelligence.

LEI WANG received the Ph.D. degree in computer applied technology from the Harbin Institute of Technology, in 2013. He is currently a Professor with the Suzhou Institute of Biomedical Engineering and Technology, Chinese Academy of Sciences, and the master's tutor with the University of Science and Technology of China. His research interests include medical decision support system for healthcare, optimization algorithm and collaborative decision-making technology based on big data analysis, and software development technology of biomedical information management systems.

QUNGANG ZHOU was born in 1973. He received the bachelor's degree from China Pharmaceutical University. In 1993, he started to work at the Suzhou Central Blood Center, engaged in quality control of blood component preparation and blood donation service. He once undertook Suzhou Science and Technology support plan and people's livelihood science and technology projects, which have been successfully concluded.